PCCP

Accepted Manuscript

This article can be cited before page numbers have been issued, to do this please use: M. Tortoza, T. D. Humphries, D. A. Sheppard, M. Paskevicius, M. R. Rowles, M. Sofianos, K. Aguey-Zinsou and C. Buckley, *Phys. Chem. Chem. Phys.*, 2017, DOI: 10.1039/C7CP07433F.

This is an Accepted Manuscript, which has been through the Royal Society of Chemistry peer review process and has been accepted for publication.

Accepted Manuscripts are published online shortly after acceptance, before technical editing, formatting and proof reading. Using this free service, authors can make their results available to the community, in citable form, before we publish the edited article. We will replace this Accepted Manuscript with the edited and formatted Advance Article as soon as it is available.

You can find more information about Accepted Manuscripts in the author guidelines.

Please note that technical editing may introduce minor changes to the text and/or graphics, which may alter content. The journal's standard Terms & Conditions and the ethical guidelines, outlined in our author and reviewer resource centre, still apply. In no event shall the Royal Society of Chemistry be held responsible for any errors or omissions in this Accepted Manuscript or any consequences arising from the use of any information it contains.

ROYAL SOCIETY OF CHEMISTRY

rsc.li/pccp

View Article Online
DOI: 10.1039/C7CP07433F

Journal Name

ARTICLE

Thermodynamics and performance of the Mg–H–F system for thermochemical energy storage applications

Received 00th January 20xx,
Accepted 00th January 20xx

DOI: 10.1039/x0xx00000x

www.rsc.org/

M. S. Tortoza,[a] T. D. Humphries,[a]* D. A. Sheppard,[a] M. Paskevicius,[a] M. R. Rowles,[a] M. V. Sofianos,[a] K. F. Aguey-Zinsou[b] and C. E. Buckley[a]

Magnesium hydride (MgH_2) is a hydrogen storage material that operates at temperatures above 300 °C. Unfortunately, magnesium sintering occurs above 420 °C, inhibiting its application as a thermal energy storage material. In this study, the substitution of fluorine for hydrogen in MgH_2 to form a range of $Mg(H_xF_{1-x})_2$ (x = 1, 0.95, 0.85, 0.70, 0.50, 0) composites has been utilised to thermodynamically stabilise the material, so it can be used as a thermochemical energy storage material that can replace molten salts in concentrating solar thermal plants. These materials have been studied by *in situ* synchrotron X-ray diffraction, differential scanning calorimetry, thermogravimetric analysis, temperature-programmed-desorption mass spectrometry and Pressure-Composition-Isothermal (PCI) analysis. Thermal analysis has determined that the thermal stability of Mg–H–F solid solutions increases proportionally with fluorine content, with $Mg(H_{0.85}F_{0.15})_2$ having a maximum rate of H_2 desorption at 434 °C, with a practical hydrogen capacity of 4.6 ± 0.2 H_2 wt% (theoretical 5.4 wt% H_2). An extremely stable $Mg(H_{0.43}F_{0.57})_2$ phase is formed upon the decomposition of each Mg–H–F composition of which the remaining H_2 is not released until above 505 °C. PCI measurements of $Mg(H_{0.85}F_{0.15})_2$ have determined the enthalpy (ΔH_{des}) to be 73.6 ± 0.2 kJ/mol H_2 and entropy (ΔS_{des}) to be 131.2 ± 0.2 J/K/mol H_2, which is slightly lower than MgH_2 with ΔH_{des} of 74.06 kJ/mol H_2 and ΔS_{des} = 133.4 J/K/mol H_2. Cycling studies of $Mg(H_{0.85}F_{0.15})_2$ over six absorption/desorption cycles between 425 and 480 °C show an increased usable cycling temperature of ~80 °C compared to bulk MgH_2, increasing the thermal operating temperatures for technological applications.

Introduction

Metal hydrides have been identified as next generation storage materials for multiple applications including hydrogen and thermal energy storage, as well as solid state electrolytes.[1-6] Magnesium hydride was first identified as a hydrogen storage material in the early 1950s with one of the first thermal decomposition studies published in 1960.[7, 8] Due to its high gravimetric hydrogen content (7.6 wt% H_2), its high volumetric storage density of 111 kg m^{-3} H_2, and the relatively low cost of magnesium, this material, and many other magnesium based metal hydrides have been identified has having potential for a variety of technologies.[9-13] To date, MgH_2 has been targeted as a stationary hydrogen storage material and thermochemical energy storage (TES) material due to its relatively high thermal stability. Upon thermal treatment at 330°C, MgH_2 decomposes into Mg and H_2 with ΔH_{des} = 74.06 kJ.mol^{-1} H_2 and ΔS_{des} = 133.4 J. K^{-1}.mol^{-1} H_2.[14]
The implementation of MgH_2 as a TES material was discussed as early as 1987 and since this time, a number of MgH_2-based hydrogen storage tanks have been developed and prototype systems manufactured.[15-21] One of the most promising applications for MgH_2 is as a TES material in concentrating solar (CSP) plants.[5, 20] The current operating temperature for a conventional CSP power plant with TES is approximately 565 °C,[22] while for next-generation CSP plants, operating temperatures between 600 °C to 800 °C are proposed.[5, 23, 24] Although the thermal properties of MgH_2 confirm that it is a good candidate as a high-temperature metal hydride (HTMH) coupled with a low-cost metal hydride pair for energy storage, the typical operating temperature (~400 °C) is not high enough to meet the targets set by industry. In addition, other contributing factors inhibit the use of pure MgH_2 as TES material due to poor cycling stability above 400 °C with a significant reduction in the H_2 storage capacity over tens to hundreds of absorption/desorption cycles due to sintering of the Mg particles.[25] Furthermore, the high H_2 equilibrium pressure of MgH_2 at 550°C, ~210 bar, makes its use impractical from an engineering perspective.[14]
The focus of the current study is to enhance the cyclic stability and to decrease the H_2 equilibrium pressure of MgH_2 by forming a solid solution between MgH_2 and MgF_2. *Sheppard et al.* recently reported that one method to increase the operating temperature of a metal hydride (*MH)* is to partially replace hydrogen by fluorine, as this thermodynamically stabilises the corresponding solid-solution metal hydride-

[a] Department of Physics and Astronomy, Fuels and Energy Technology Institute, Curtin University, GPO Box U1987, Perth, WA 6845, Australia. E-mail: terry_humphries81@hotmail.com
[b] Merlin Group, School of Chemical Engineering, The University of New South Wales, Sydney, NSW 2052, Australia.
†Electronic Supplementary Information (ESI) available: XRD analysis of ball milled and annealed $Mg(H_xF_{1-x})_2$-*L* samples; DSC-TGA-MS analysis of $Mg(H_xF_{1-x})_2$-*L* samples; summary of PCI data for $Mg(H_{0.85}F_{0.15})_2$. See DOI: 10.1039/x0xx00000x

View Article Online
DOI: 10.1039/C7CP07433F

fluoride.[26-28] As such, many materials that operate below the target temperature of ~500 °C may become feasible for higher temperature applications. Furthermore, the addition of fluorine can reduce the cost of a TES system and improve metal hydride reversibility, which is a key factor given the typical 30-year lifetime of a CSP plant.[27, 29]

To increase the operating temperature of the Mg–H system, fluorine substitution to form $Mg(H_xF_{1-x})_2$ solid solutions have been studied herein. Previous studies on mixtures of MgH_2 + xMF_y (M = Mg, Zr, Ti, Fe, Ta, Ni, Nb; x = 5 - 7 mol%; y = 2 - 5) have concentrated on improving the kinetics of MgH_2 for operation at lower temperatures.[30-35] The kinetics of decomposition were determined to be considerably faster than pure MgH_2 with full H_2 release within 600 s,[30] with negligible loss in H_2 cycling capacity at 310 °C. The reason for the improved kinetics has been explored by a variety of techniques including X-ray photoemission spectroscopy (XPS) and powder X-ray diffraction (XRD),[33, 34] although there are mixed reports on whether the transition metal or MgF_2 species formed is responsible for the enhanced performance.[30, 33, 34] Recently a preliminary study has shown that MgH_2 and MgF_2 forms solid solutions with $Mg(H_{0.9}F_{0.1})_2$ reversibly absorbing 5.5 wt % H_2 in less than 3 min at 440 °C.[36] Thermal analysis by differential scanning calorimetry (DSC) indicates that ΔH_{des} for $Mg(H_{0.9}F_{0.1})_2$ is close to that of MgH_2 (74.0 kJ.mol^{-1} H_2),[14] and decreases with decreasing H content. However, without the determination of ΔS_{des} the stability of the material can't be truly assessed. Previous studies have shown that incremental substitution of F causes a decrease in ΔH_{des} although a concomitant decrease in ΔS_{des} causes an overall stabilisation of the material.[27] Further analysis of this system by pressure-composition-isotherm (PCI) analysis is required to precisely determine the decomposition pathway and the associated thermodynamics. These properties are required to assess the viability of $Mg(H_xF_{1-x})_2$ as a TES material, especially at temperatures > 400 °C.

In this study, MgH_2 has been ball-milled with MgF_2 followed by annealing to successfully form solid solutions of $Mg(H_xF_{1-x})_2$ (x = 1, 0.95, 0.85, 0.70, 0.50, 0) to determine differences in their structural and thermodynamic properties. Time resolved synchrotron radiation powder X-ray diffraction (SR-XRD) studies have been carried out on a range of $Mg(H_xF_{1-x})_2$ compositions to ascertain the differences in thermal decomposition pathways of these compounds. The thermodynamic and kinetic properties of these solid solutions have been determined by PCI analysis using the van't Hoff method, differential scanning calorimetry (DSC), thermogravimetric analysis (TGA), temperature-programmed-desorption mass spectrometry (TPD-MS). Cycling studies have also been carried out to determine the feasibility of the Mg–H–F system for CSP application.

Experimental

All manipulations of chemicals were undertaken in an argon atmosphere using an Mbraun Unilab glovebox to prevent air exposure and to minimise oxygen (O_2 < 1 ppm) and water (H_2O < 1 ppm) contamination. $Mg(H_xF_{1-x})_2$ (x = 1, 0.95, 0.85, 0.70, 0.50, 0) samples were prepared by ball milling (BM) various ratios (Table 1) of MgH_2 and MgF_2 (Sigma-Aldrich, >99.99 %) at room temperature. MgH_2 powder (95 wt% purity from Rietveld refinement) was first synthesised by annealing Mg powder (Aldrich, >99 %) at 400 °C under 30 bar hydrogen pressure for 18 hours. The partially hydrogenated Mg was then BM for 3 hours with a ball-to-powder mass ratio of 10:1 in a Shaker Mill (Turbula T2C shaker-mixer) and annealed once again under identical conditions (400 °C, 30 bar H_2, 18 h). BM of MgH_2 and MgF_2 was undertaken at 400 rpm for 10 hours (labelled *S*) or 40 hours (labelled *L*) in an Across International Planetary Ball Mill (PQ-N04) with a ball-to-powder mass ratio of 50:1 using stainless steel vials and balls (6 and 8 mm in diameter) under an Ar atmosphere. After milling, samples were annealed under a hydrogen atmosphere of 60 bar at 450 °C for a period of 90 hours to form uniform solid solutions. Annealing samples under H_2 prevents hydrogen release from the material.[27]

Before and after annealing the $Mg(H_xF_{1-x})_2$ powders, quantitative phase analysis was undertaken by conducting *ex situ* XRD analysis on each sample. The powders were mixed with ~10 wt% Si (−325 mesh, Aldrich) as an internal standard (a = 5.42960(4) Å), used to extract reliable lattice parameters for the solid solutions. *Ex situ* XRD was performed using a Bruker D8 Advance diffractometer (Cu-$K_{\alpha 1+2}$ radiation, λ = 1.5418 Å) with flat-plate sample holders sealed by a polymethylmethacrylate (PMMA) dome in order to prevent oxygen/moisture contamination during data collection. The PMMA dome resulted in a broad hump in XRD patterns centred at ~20° 2ϑ. Acquisition of data was subsequently restricted to 2ϑ = 20 − 80°, with a $\Delta 2\vartheta$ = 0.02° and 2 s/step scanning rate with a sample rotation rate of 60 rpm.

In situ synchrotron radiation SR-XRD was performed at the Australian Synchrotron in Melbourne, Australia.[37] Without exposure to air, the $Mg(H_xF_{1-x})_2$ powders (ball milled for 40 h) were loaded into borosilicate or quartz capillaries (outer diameter 0.7 mm, wall thickness 0.01 mm) that were then, using graphite ferrules, mounted in 1/16″ tube fittings connected to a gas manifold. The samples were kept under dynamic vacuum while heated with a hot air blower up to 615 °C (Room Temperature (RT) → 200 °C at 10 °C/min, 200 → 615 °C at 5 °C/min). $Mg(H_{0.50}F_{0.50})_2$ was measured with a temperature heating rate of 8 °C/min from 150 to 785 °C. One-dimensional SR-XRD patterns (monochromatic X-rays with λ = 1.000389(1), 0.826307(1) or 0.774541(1) Å) were collected using a Mythen microstrip detector with an exposure time of 54 s per pattern. The capillaries were continuously oscillated through 120° during exposure to improve powder averaging. Diffraction patterns were quantitatively analysed using the Rietveld refinement method with TOPAS software (Bruker-AXS). The temperature of the hot-air blower was calibrated against the known thermal expansion coefficients for NaCl and Ag.[38, 39]

TGA and DSC in conjunction with MS (DSC-TGA-MS) analyses were conducted using sample masses of ~10 mg at a heating rate of 10 °C/min under an argon flow of 20 mL/min using a Mettler Toledo TGA/DSC 1 coupled with an Omnistar MS.

View Article Online
DOI: 10.1039/C7CP07433F

Journal Name

ARTICLE

Table 1. Structural properties of $Mg(H_xF_{1-x})_2$-*L* mixtures (*P*42/*mnm*) at room temperature. Estimated standard deviations (esd's) of lattice parameters and H occupancies in the 4*f* site are in parentheses.

Sample Name	MgH_2:MgF_2 Molar ratio (target)	Lattice Parameter (Å) *a*	*c*	H Occupancy	Unit cell volume (Å^3)	Mg_2FeH_6 impurity (wt%)	Theoretical H_2 capacity excluding Mg_2FeH_6 content (wt%)
MgH_2	1:0	4.51746(5)	3.02215(6)	1(0)	61.674(2)	0	7.66
$Mg(H_{0.95}F_{0.05})_2$	0.95:0.05	4.52109(4)	3.02306(4)	0.919(9)	61.792(1)	0	6.81
$Mg(H_{0.85}F_{0.15})_2$	0.85:0.15	4.54238(6)	3.029517(7)	0.801(2)	62.509(0)	3	5.40
$Mg(H_{0.70}F_{0.30})_2$	0.7:0.3	4.55932(3)	3.03417(3)	0.727(5)	63.072(1)	7	3.80
$Mg(H_{0.50}F_{0.50})_2$	0.5:0.5	4.59133(2)	3.04372(2)	0.393(4)	64.162(1)	12	2.27
MgF_2	0:1	4.62312(2)	3.05195(2)	0(0)	65.230(1)	0	---

Masses (*m*/*e* = 2 – 100) were monitored up to 550 °C, however the $Mg(H_{0.50}F_{0.50})_2$ was measured up to 850 °C. The instrument was installed in an Ar filled glovebox to avoid air contamination during sample handling. The temperature accuracy of this instrument is ±0.2 °C, while the balance has an accuracy of ±20 µg.

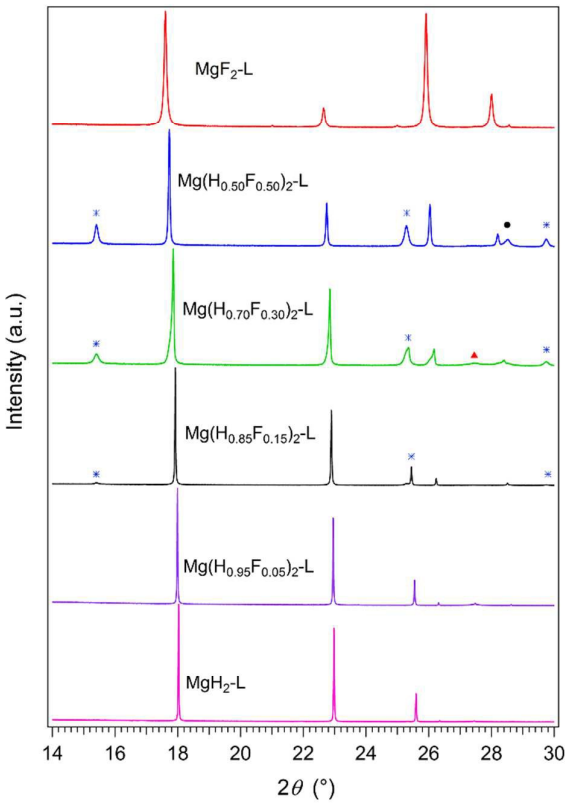

Fig. 1. *In situ* SR-XRD at room temperature of $Mg(H_xF_{1-x})_2$ samples ball milled for 40 hours and annealed. * signifies Mg_2FeH_6, ● signifies Fe and ▲signifies MgO. All other Bragg peaks are associated with the $Mg(H_xF_{1-x})_2$ mixtures. λ = 1.000389(1) Å.

All hydrogen absorption/desorption measurements were performed by using a computer controlled Sieverts/volumetric apparatus previously described elsewhere.[14] The digital pressure transducer (Rosemount 3051S) had a precision and accuracy of 14 mbar, whilst room temperature measurements were recorded using a 4-wire platinum resistance temperature detector (RTD). Isothermal PCI curves were performed at 437, 444, 450 and 461 °C and monitored by a K-type thermocouple (± 4 °C). Above ~420 °C, the permeation of hydrogen directly through the walls of the stainless steel sample cell becomes an issue and the measured hydrogen content at each PCI data point has to be corrected for this loss, as previously explained.[28] In addition, hydrogen absorption PCI measurements were carried out at ~450 °C on the same apparatus.

Hydrogen absorption/desorption cycles were conducted by heating a sample of $Mg(H_{0.85}F_{0.15})_2$ at 4 °C/min from room temperature to 425 °C followed by a 6 h isothermal period. The temperature was then heated at 2 °C/min to 480 °C followed by another 6 h isothermal step; it is during this stage the first decomposition begins. The temperature was then cycled between 425 °C (hydrogen absorption) and 480 °C (hydrogen desorption) 6 times under a closed gas system pressure varying between 30 - 42 bar.

Results and Discussion

Structure and Composition.

View Article Online
DOI: 10.1039/C7CP07433F

The BM powders were analysed by *ex situ* XRD before and after annealing to confirm that a $Mg(H_xF_{1-x})_2$ solid solution was formed and that neither of the MgH_2 and MgF_2 starting materials were present (Fig. S1). Due to the fact that MgH_2 and MgF_2 both exist in a tetragonal rutile crystal structure (*P*42/*mnm*),[40, 41] the solid solutions of $Mg(H_xF_{1-x})_2$ also possess identical structures, as predicted by Messer.[42] The annealing process, while also enhancing the crystallinity of the samples, was necessary to allow the H and F atoms to substitute in to the 4*f* sites and form a uniform solid solution (Table 1). Milling alone is not enough to facilitate the formation of a uniform single phase, although extended milling time aids in attaining a uniform sample composition. However, extended milling may lead to the introduction of iron impurities from the stainless-steel canisters and balls, resulting in the formation of small amounts of Mg_2FeH_6 being evident after annealing (Fig. 1, Table 1).[43, 44] Therefore, it is important to restrict long milling times in order to reduce the quantity of impurities. After BM for 40 h the samples were analysed by XRD and it can be seen that the samples exhibit broad diffraction peaks suggestive of a single tetragonal phase or an extended range of $Mg(H_xF_{1-x})_2$ compositions (Fig. S1), but annealing promotes crystallisation into single phase compositions (Fig. 1). Quantitative phase analysis of each the mixtures identifies that $Mg(H_{0.50}F_{0.50})_2$-*L* contains the largest quantity of Mg_2FeH_6 [43, 44] (Table 1) and it is deemed that the greater hardness of MgF_2 compared to stainless-steel is responsible (MgF_2 has a hardness of 415 kg/mm^2 Knoop,[45] whereas stainless steel has a hardness of 166 kg/mm^2 Knoop).[46] Therefore, increased MgF_2 content in the sample promotes erosion of the stainless steel and, by consequence, incremental quantities of Mg_2FeH_6 are observed. In addition, Fe metal is observed in only the $Mg(H_{0.50}F_{0.50})_2$-*L* materials. Some MgO is observed in sample $Mg(H_{0.70}F_{0.30})_2$-*L* due to an inadvertent exposure of the sample to air during mounting of the capillary before XRD. MgO and other impurities may also be formed due to reaction with the borosilicate or quartz capillaries. In this study, no additional impurity phases were identified to form during the in situ heating experiment.

Fig. 1 illustrates the SR-XRD patterns for each of the *L*-solid solutions at room temperature. It is noted that the peaks for $Mg(H_xF_{1-x})_2$ move to lower angles (higher *d*-spacing) with increased F content. This is emphasised in Fig. S2. This shift causes a concomitant increase in unit cell volume from 61.674(2) Å^3 for MgH_2 to 65.230(1) Å^3 for MgF_2 (Table 1). This is expected due to the longer Mg–F bond distances of 1.9968 Å[47] in MgF_2 compared to the apical Mg–H distance of 1.94(2) Å and the equatorial Mg–H distance of 1.97(2) Å in MgH_2.[48] The lattice parameters for the Mg–H–F solid solution are illustrated in Fig. 2a and clearly show that the *a* and *c* parameters increase with increasing fluorine content, with *a* having a dominant influence on the unit cell expansion. Previous studies have used the lattice parameters to predict the H/F compositions of the materials after hydrogen absorption/desorption cycles,[27] while the unit cell volume can also be utilised (Fig. 2b). The H occupancy factor may also be employed as a measure of substitution between H and F (Fig. 2b). Despite H having a negligible scattering factor, the X-ray cross section of F allows for appreciable determination of the occupancy of the 4*f* site of which the F and H share.

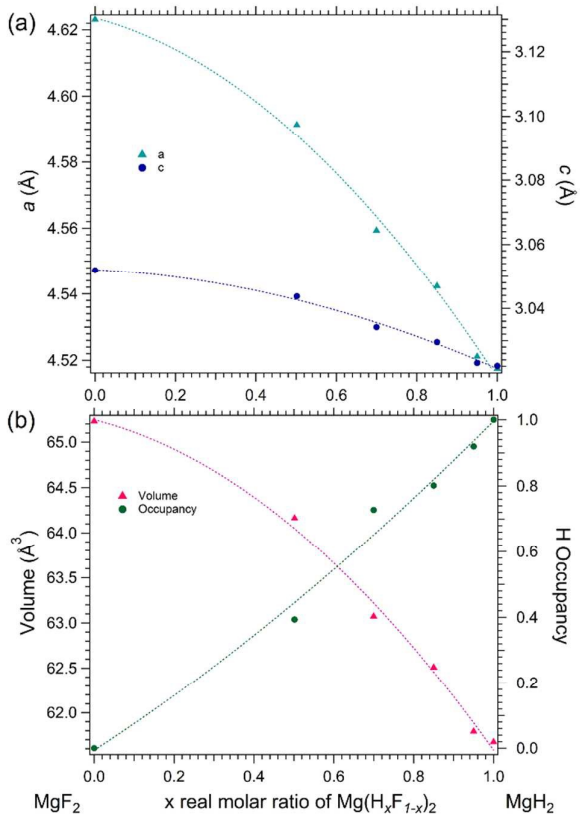

Fig. 2. Refined lattice parameters of $Mg(H_xF_{1-x})_2$-*L* mixtures from room temperature *in situ* SR-XRD. (a) Quadratic fit for lattice parameters *a* and *c* versus composition. $a = -0.0762x^2 - 0.0326x + 4.6236$. $c = -0.0239x^2 - 0.0069x + 3.0521$ (b) quadratic fit for unit cell volume and H occupancy versus composition. Unit cell volume $V = -2.5527x^2 - 1.1113x + 65.246$. H Occupancy $= 0.2073x^2 + 0.7952x - 0.0064$.

To avoid Fe impurities the milling time of the samples were reduced to 10 h while maintaining the annealing conditions (90 h at 450 °C at 60 bar H_2). These samples are labelled as $Mg(H_xF_{1-x})_2$-*S*. The annealed *S* samples were analysed by XRD and show no presence of Mg_2FeH_6 although the shape of the $Mg(H_xF_{1-x})_2$ solid solution Bragg peaks were asymmetric (Fig. S3).

Thermal analysis.

In situ SR-XRD was carried out up to 615 °C on all sample compositions with Fig. 3a illustrating $Mg(H_{0.85}F_{0.15})_2$ and exemplifying the decomposition process (also see Fig. S4-S6). As temperature increases, thermal expansion causes the lattice parameters of $Mg(H_{0.85}F_{0.15})_2$ (and the minor Mg_2FeH_6 phase) to expand (2ϑ decreases) before both materials decompose simultaneously at an onset temperature of 433 °C with total decomposition occurring by 440 °C. The decomposition observed in XRD data is also mirrored in the TGA-DSC-MS data (Fig. 3b - d). The DSC data show a single endothermic event between 350 - 450 °C for all hydrogen

View Article Online
DOI: 10.1039/C7CP07433F

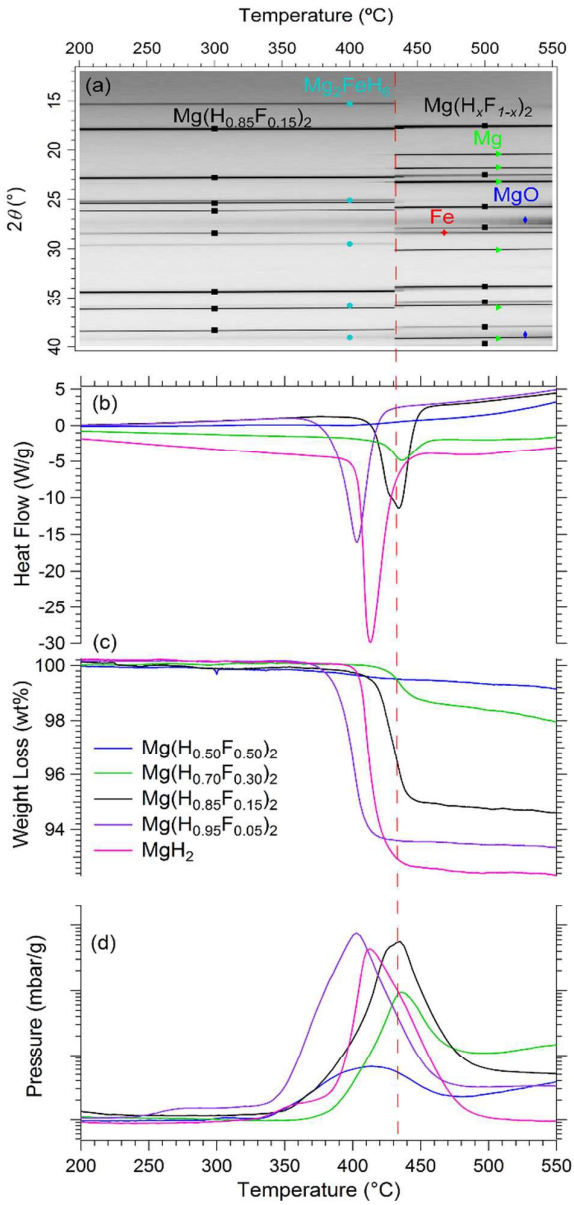

Fig. 3. (a) *In situ* XRD for $Mg(H_{0.85}F_{0.15})$. λ = 1.000389(1) Å. Simultaneous thermal analysis of $Mg(H_xF_{1-x})_2$ samples by (b) DSC, (c) TGA and (d) MS. $\Delta T/\Delta t$ = 10 °C/min. DSC and MS data are normalised to the mass of the sample.

containing samples (Fig. 3b, Table 2). The onset temperature for the decomposition of pure MgH_2-*S* is ~394 °C with a maximum H_2 release at ~413 °C. The decomposition temperature of the pure hydride is greater than that of $Mg(H_{0.95}F_{0.05})_2$-*S*, which has on onset temperature of 360 °C and a maximum H_2 release temperature of 405 °C. From this it can be inferred that $Mg(H_{0.95}F_{0.05})_2$-*S* has faster kinetics of desorption than pure MgH_2-*S*, a result that has also been noted previously.[32] Further substitution of H by F appears to kinetically and/or thermodynamically stabilise MgH_2 with $Mg(H_{0.85}F_{0.15})_2$-*S* having a decomposition onset of 405 °C (peak maximum of 434 °C), while $Mg(H_{0.70}F_{0.30})_2$-*S* has an onset of ~415 °C (peak maximum of 437 °C). One of the most intriguing results is that $Mg(H_{0.50}F_{0.50})_2$-*S* shows no obvious decomposition event during DSC measurement up to 550 °C (Fig. 3b). This is in agreement with the *in situ* SR-XRD measurement of $Mg(H_{0.5}F_{0.50})_2$-*L* up to 615°C, Fig. S5. This particular *in situ* SR-XRD pattern also shows the presence of Mg_2FeH_6, which disappears at ~450 °C in conjunction with the appearance of Mg at the same temperature. The disappearance of the Mg at ~530 °C is due to the migration of Mg vapour from the hot-zone during measurement.

The decomposition onset for the Mg_2FeH_6 impurity phase determined in each of the $Mg(H_xF_{1-x})_2$ (x = 0.85, 0.70, 0.50) samples measured by *in situ* XRD occurs at ~430 °C. A previous *in situ* XRD decomposition study of Mg_2FeH_6 shows the onset of decomposition to occur at ~340 °C under 1 bar Ar.[49] To ascertain if F substitution had occurred within Mg_2FeH_6 during annealing, refinement of the lattice parameter and H/F occupancy factors on the 24*e* site in the $Fm\bar{3}m$ unit cell was undertaken. At room temperature the unit cell dimension was determined as 6.46277(8) Å, which is only 0.25% larger than 6.44686(2) Å determined in a previous study,[50] while the hydrogen occupancy was refined to be 100%. At ~380°C the hydrogen occupancy was determined to be 96.8(9) %, which indicates that some F substitution may have occurred at higher temperatures, and in turn may have increased the thermal stability of the Mg_2FeH_6 material.

DSC and TPD-MS data were also collected for the samples milled for 40 h (*L*, Fig. S7). Upon comparing the *L* and *S* samples measured by DSC, it appears that extended milling times reduce the observed temperature of the endothermic peak compared to the corresponding compositions milled for 10 h. For instance, the maximum rate of H_2 release for $Mg(H_{0.70}F_{0.30})_2$-*S* is 437 °C, whereas it is 367 °C for $Mg(H_{0.70}F_{0.30})_2$-*L*. Extended milling decreases the crystallite and particle size, decreases diffusion pathways, increases the specific surface area and introduces defects. All of these factors contribute to faster kinetics that allow the hydride to decompose at a lower temperature.[14]

TPD-MS was used to analyse the gases released by materials upon thermal treatment. In this study, the gases released during DSC-TGA were analysed for all *m*/*e* up to 100 showing that only H_2 was released during thermal treatment (Fig. 3d, log scale). The most striking result is that for $Mg(H_{0.50}F_{0.50})_2$-*S* only minor H_2 evolution is observed between 290 and 475 °C. In fact, all samples apart from $Mg(H_{0.70}F_{0.30})_2$-*S* start to desorb hydrogen between 290 and 340 °C, while it is only the peak rate of release that differs between the samples.

Considering that the thermal analysis experiments have indicated that increasing the F content in the samples increases thermal stability compared to pure MgH_2, it would be assumed that the $Mg(H_{0.50}F_{0.50})_2$ sample would be the ideal candidate for further studies as a HTMH for TES applications. However, the larger practical hydrogen capacity of $Mg(H_{0.85}F_{0.15})_2$ is far greater than $Mg(H_{0.50}F_{0.50})_2$ below 550 °C (5.06 ± 0.02 wt% H_2 and 0.77 ± 0.01 wt% H_2, respectively). As such, $Mg(H_{0.85}F_{0.15})_2$-*S* was deemed an ideal candidate to be studied by PCI between 437 and 461 °C to determine its thermodynamics of

View Article Online
DOI: 10.1039/C7CP07433F

Journal Name

ARTICLE

Table 2. Decomposition temperatures and hydrogen capacities and values of $Mg(H_xF_{1-x})_2$-*S* mixtures measured by DSC-TGA up to 550 °C. $\Delta T/\Delta t$ = 10 °C/min.

Sample	Practical / theoretical H_2 capacity (TGA, wt %)	Hydrogen yield (%)	Onset/Peak Temperature of H_2 desorption (DSC, °C) *	Temperature in middle point of step (TGA, °C) *	Peak Temperature of H_2 desorption (MS, °C) *
MgH_2	7.50 ± 0.03 / 7.66	97.9	394/413	413	412
$Mg(H_{0.95}F_{0.05})_2$	6.60 ± 0.03 / 6.81	96.9	360/405	400	403
$Mg(H_{0.85}F_{0.15})_2$	5.06 ± 0.02 / 5.4	93.7	405/434	430	435
$Mg(H_{0.70}F_{0.30})_2$	1.60 ± 0.01 / 3.8	42.1	415/437	433	436
$Mg(H_{0.50}F_{0.50})_2$	0.77 ± 0.01 / 2.27	33.9	---	---	~414

* Temperature reported as integers although accurate to 0.02 °C.

decomposition (Fig. 4a). The PCI curves in Fig. 4a show that decomposition follows a single step process that releases an average total of 4.6 ± 0.2 wt% H_2 for the four temperatures measured, with equilibrium pressures between 32 and 38 bar. Each of the curves exhibits a sloping plateau that is highly characteristic of a solid solution of this type, albeit not as sloped as those observed in the $NaH_{0.50}F_{0.50}$ or $NaMgH_2F$ systems.[27, 28] Sloping plateaus are not ideal in practical applications due to the fact that hydrogen absorption and desorption does not occur in an isobaric process,[28] and the range of operational system pressures over the equilibrium transition becomes larger.

Generally, the thermodynamics of absorption/desorption are determined by measuring the pressure at the midpoint of the equilibrium plateau and plotting this as a function of temperature in a van't Hoff plot. In this study, due to the sloping plateau, each of the four curves were numerically fitted throughout the plateau region so that the enthalpy and entropy could be determined at any hydrogen content (Fig. 4).[28] All of the information obtained from the PCI measurements presented in Fig. 4, are summarised in Table 3. The enthalpy (ΔH_{des}) and entropy (ΔS_{des}) of hydrogen desorption are also presented in Table 3. The uncertainties for the data were calculated using the weighted least squares method with a 95% confidence interval as described in previous work.[14] The enthalpy, ΔH_{des}, decreases from 74.7 to 72.2 kJ/mol H_2 between −1 wt% to −3 wt% H_2 desorption. With regards to entropy, these values also show the same trend, decreasing in value from 133.0 to 129.1 J/K/mol H_2. This means that at −2 wt% H_2 (middle point of the plateau), ΔH_{des} = 73.6 ± 0.2 kJ/mol H_2 and ΔS_{des} = 131.2 ± 0.2 J/K/mol H_2, are 0.66% and 1.65% lower than that of pure

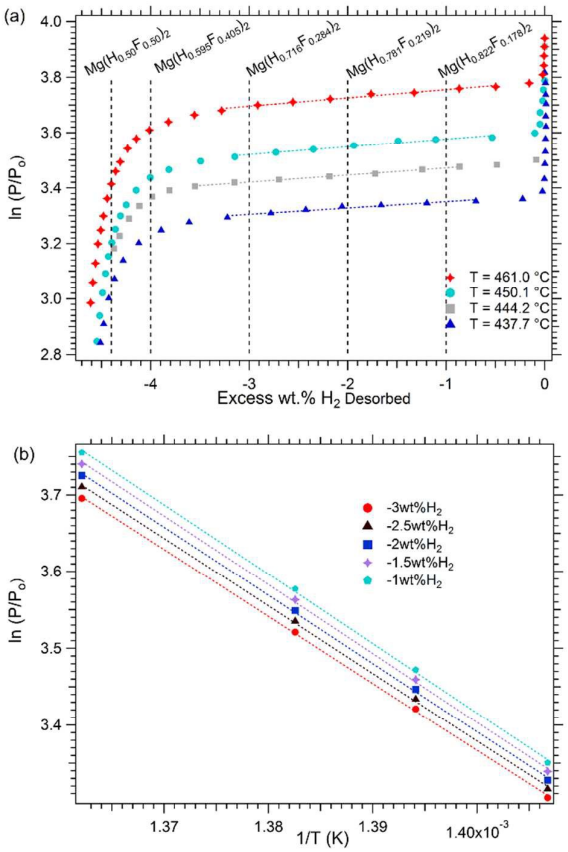

Fig. 4. (a) Pressure–Composition-Isotherms (PCI) for $Mg(H_{0.85}F_{0.15})_2$-*S* performed between 437 °C and 461°C. ♦ln $(P/P_o)_{461°C}$= 0.02978 *x* + 3.7850, ●ln $(P/P_o)_{450.1°C}$ = 0.0279*x* + 3.6048, ▪ln $(P/P_o)_{444.2°C}$ = 0.0256*x* + 3.4978, ▲ln $(P/P_o)_{436°C}$ = 0.0227*x* + 3.3731, where *x* = wt% H_2 desorbed. (b) van't Hoff plot of respective H_2 desorption equilibrium pressures, where *T* is temperature (K). P_o=1 bar.

View Article Online
DOI: 10.1039/C7CP07433F

Journal Name

ARTICLE

Table 3. Thermodynamic properties at 5 different hydrogen contents for $Mg(H_{0.85}F_{0.15})_2$-*S*

At H_2 wt%	ΔH_{des} (kJ/mol H_2)	ΔS_{des} (J/K/mol H_2)	ΔG (J/mol H_2)	van't Hoff plot ln(*P*/*Po*)
−1	74.7 ± 0.2	133.0 ± 0.3	21.2 ± 0.2	−8982/T + 15.99
−1.5	74.1 ± 0.2	132.1 ± 0.2	21.2 ± 0.2	−8916/T+15.87
−2	73.6 ± 0.2	131.2 ± 0.2	21.1 ± 0.2	−8849/T+15.78
−2.5	72.9 ± 0.2	130.2 ± 0.3	21.0 ± 0.2	−8772/T+15.66
−3	72.2 ± 0.2	129.1 ± 0.3	20.9 ± 0.2	−8685/T+15.53
Pure MgH_2*	74.06	133.4	22.17	---

*ref [14]

MgH_2, respectively. This indicates that the equilibrium pressure at which decomposition will occur is insignificantly lower than that for MgH_2 at the same temperature. However, along the plateau the equilibrium pressures change (due to the sloping plateau) resulting in ΔH_{des} ($Mg(H_{0.85}F_{0.15})_2$-*S*) > ΔH_{des} MgH_2 while < −1.58 wt%, and after this point (> −1.58 wt%) ΔH ($Mg(H_{0.85}F_{0.15})_2$-*S*) < ΔH MgH_2. However, ΔS_{des} ($Mg(H_{0.85}F_{0.15})_2$-*S*) < ΔS_{des} MgH_2 *all along the plateau*. Although these are only small changes in ΔH and ΔS, it is still significant and are linked

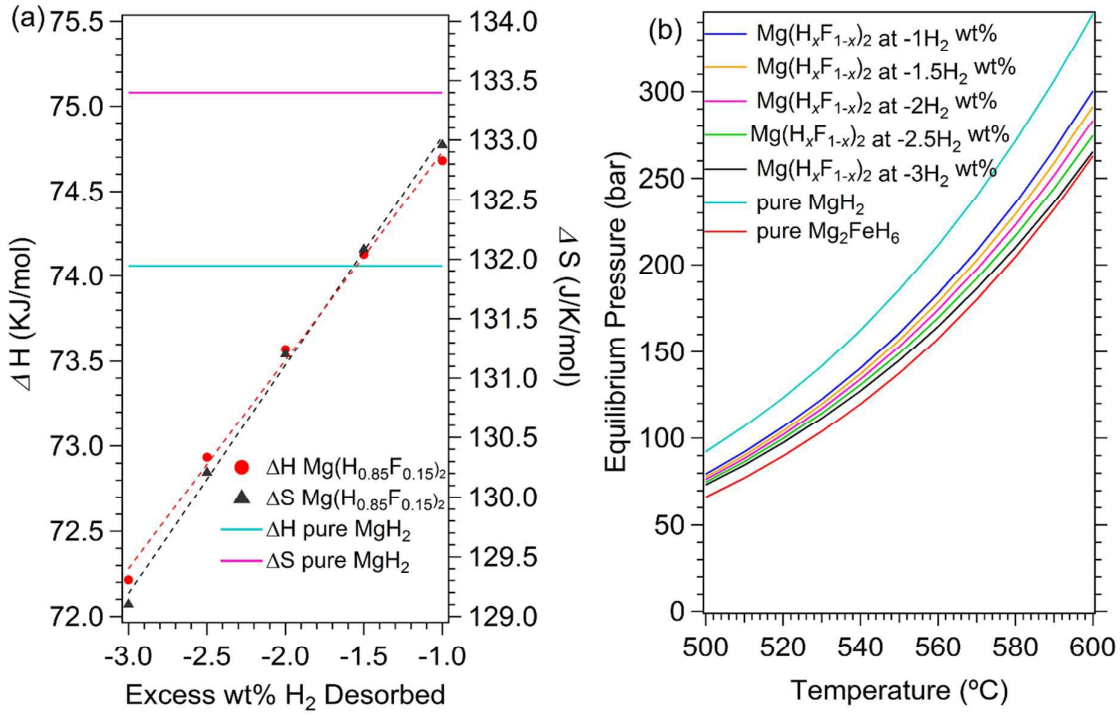

Fig. 5. (a) Reaction enthalpy and entropy for $Mg(H_{0.85}F_{0.15})_2$. ΔS_{des} = 1.9181 × (wt% H_2) + 134.95, ΔH_{des} = 1.225 × (wt% H_2) + 75.995 (b) Predicted equilibrium pressures of MgH_2 and $Mg(H_{0.85}F_{0.15})_2$ at 5 different values of H_2 wt% along the equilibrium plateau. For Fig 5b: pure MgH_2[14] and Mg_2FeH_6.[44]

View Article Online
DOI: 10.1039/C7CP07433F

Journal Name

ARTICLE

with the sloping nature of the plateau. Frequently, a flat equilibrium plateau is observed when a material decomposes into another with a different crystal structure. In this particular case, the same space group, *P*42/*mnm,* is shared for both the starting and final products. As a consequence, it is observed that during PCI experiments, H_2 is progressively desorbed allowing an F rich phase to emerge. This F-rich phase also possesses the same crystal structure, allowing for changes to occur gradually, which explains the nature of the sloping plateau. For this reason, the thermodynamics of decomposition change gradually during the measurement. It needs to be mentioned that ΔG for hydrogen release from $Mg(H_{0.85}F_{0.15})_2$ is equivalent to ΔG for hydrogen release from MgH_2, therefore $\Delta G = 0$ (1 bar equilibrium temperature) is at 273.7 °C for both $Mg(H_{0.85}F_{0.15})_2$ and MgH_2 within experimental uncertainty.

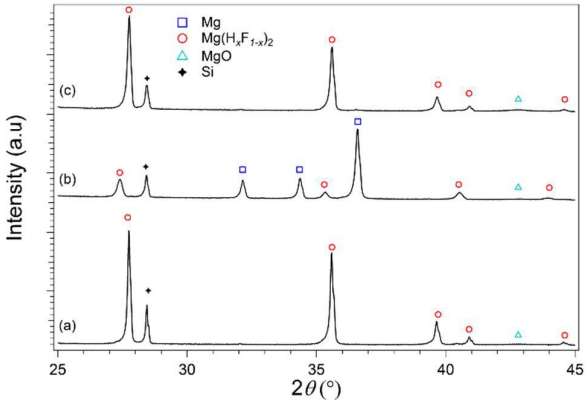

Fig. 6. (a) *Ex situ* XRD of $Mg(H_{0.85}F_{0.15})_2$; (b) after PCI desorption at 450 °C; (c) after PCI absorption at 450 °C. λ = 1.5418 Å, at room temperature.

Figure 5b also shows that the H_2 equilibrium pressures of the $Mg(H_xF_{1-x})_2$ decreases and moves closer to that of Mg_2FeH_6 as the temperature increases. It should be noted that during PCI measurements the quantity of desorbed H_2 for $Mg(H_{0.85}F_{0.15})_2$ (4.6 wt% H_2, Table S1) did not reached the theoretical hydrogen capacity of 5.4 wt%. This can be attributed to the formation of a stable Mg–H–F phase. An XRD pattern of $Mg(H_{0.85}F_{0.15})_2$-*S* was measured before and after the PCI test (Fig. 6 a and b), after PCI desorption at 450 °C XRD confirmed that $Mg(H_xF_{1-x})_2$ was present, supporting the hypothesis of a stable Mg–H–F phase. This finding correlates well with the high stability observed for $Mg(H_{0.50}F_{0.50})_2$ during thermal analysis by *in situ* SR-XRD and DSC-TGA-MS. Rietveld refinement of the XRD pattern to determine the unit cell volume provides a composition of $Mg(H_{0.43}F_{0.57})_2$, also corresponding to the fact that ~0.8 wt% H_2 remains within the sample (Table S1).

The thermal stability of the $Mg(H_{0.50}F_{0.50})_2$-*L* composition was subsequently investigated by TGA-MS and *in* situ SR-XRD up to 850 °C to determine the temperature at which the remaining H_2 could be desorbed (Fig. S8 and S9). As noted previously, during TGA measurement (Fig. 3c) of $Mg(H_{0.50}F_{0.50})_2$, before 480 °C only 0.77 wt% H_2 is desorbed, but after 505 °C a major desorption event occurs (Fig. S8) releasing a total mass loss of 2.3 wt% before 830 °C. This value is slightly greater than the theoretical quantity of 2.27 wt % H_2 as Mg evaporates at this temperature due to its low vapour pressure. The first step of decomposition, observed at ~400 °C during TGA-MS, Fig. S8, is not clearly witnessed by *in situ* SR-XRD but at ~545 °C a significant expansion of the unit cell is observed, beyond that expected from of thermal expansion alone (Fig. S9). At the same time, the peaks become broader and asymmetric in shape. This is most likely a consequence of a variety of solid-solution compositions being present during decomposition. At ~755 °C the hydrogen occupancy factor is 2.9(5) % indicating that full decomposition has almost been achieved under vacuum conditions.

The high thermal stability of the $Mg(H_{0.43}F_{0.57})_2$ composition may permit this material to be implemented as a TES material as it will operate at above 600 °C, which is above the operating temperature currently achievable using molten salts of 565 °C.[23] The evaporation of Mg at high temperatures is a major concern as upon decomposition, 22.7 wt% of Mg metal is formed. Over time, this will lead to a major decrease in capacity unless a method of inhibiting segregation is utilised. One such method, previously used in studies of Na/NaH at temperatures of up to 900 °C and H_2 pressures of 650 bar, is to enclose the sample in thin Fe tubing or foil.[51] The extreme thermal stability of this material should be investigated by theoretical methods to understand the unexpected thermodynamic stability, while the thermodynamic properties should also be determined experimentally.

Overall, each method of thermal analysis used in this study illustrates that the thermal stability of the Mg–H–F systems increase with addition of F. A previous report on this system mentions that data measured by DSC indicates a destabilisation due to a decrease in ΔH_{des}.[36] As stated above, ΔS_{des} is required to ultimately determine the overall stability of the system. This study shows that for $Mg(H_{0.85}F_{0.15})_2$, a concomitant decrease in ΔS_{des} is observed during addition of F to the mixture, which causes an overall increase in stability. This pattern has been established previously during the study of Na–H–F in which PCI measurements determined a ΔH_{des} of 106 ± 5 kJ·mol^{-1} H_2 and ΔS_{des} of 143 ± 5 J·K^{-1}·mol^{-1} H_2 for

View Article Online
DOI: 10.1039/C7CP07433F

$NaH_{0.50}F_{0.50}$ compared to 117 kJ·mol^{-1} H_2 and 167 J·K^{-1}·mol^{-1} H_2 for pure NaH.[27]

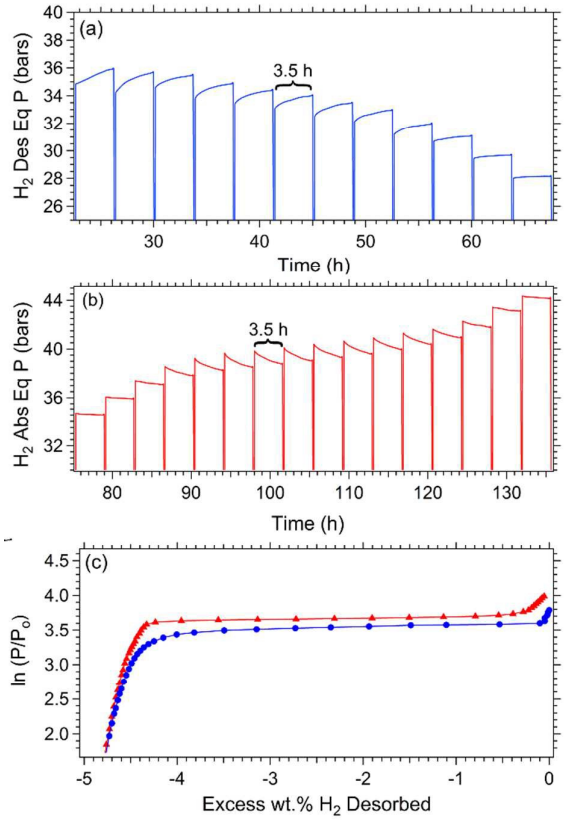

Fig. 8. (a) Hydrogen desorption kinetic data for the PCI of $Mg(H_{0.85}F_{0.15})_2$ performed at 450 °C, (b) Hydrogen absorption kinetic data for the PCI of $Mg(H_{0.85}F_{0.15})_2$ performed at 450 °C; (c) Hydrogen desorption (●) and absorption (▲) PCIs performed at 450 °C.

Rehydrogenation studies

In order for $Mg(H_{0.85}F_{0.15})_2$ to be considered as potential material for hydrogen storage or thermal energy storage applications, characteristics such as hysteresis (absorption/desorption pressure), cyclic stability and reversibility need to be assessed.[14, 21] After the PCI measurement at 450 °C (Fig. 7a), a hydrogen absorption experiment was performed on the sample
at the same temperature (450 °C) (Fig. 7b). An initial pressure of 3 bar was increased to 55 bar in a step-wise fashion, with 3.5 h equilibrium step times (identical to desorption measurements). According to the ΔH_{des} and ΔS_{des} for $Mg(H_{0.85}F_{0.15})_2$ determined by PCI, the sample is predicted to start absorbing H_2 at an equilibrium pressure of ~34 bar (Fig. 7b). As observed in Fig. 7c, the sample starts to absorb a significant amount of H_2 above ~36 bar. Figures 7a and 7b represent the kinetic data for desorption and absorption, respectively. These graphs show that $Mg(H_{0.85}F_{0.15})_2$ does not reach true equilibrium after 3.5 h, indicating that reaction kinetics during absorption are appreciably slower than observed during dehydrogenation. If a longer equilibration step time was afforded for each step then hysteresis may not be observed. Despite the kinetics of absorption being slow, the sample absorbed ~98% of the hydrogen that was previously desorbed and equates to ~88% of the theoretical value. At the

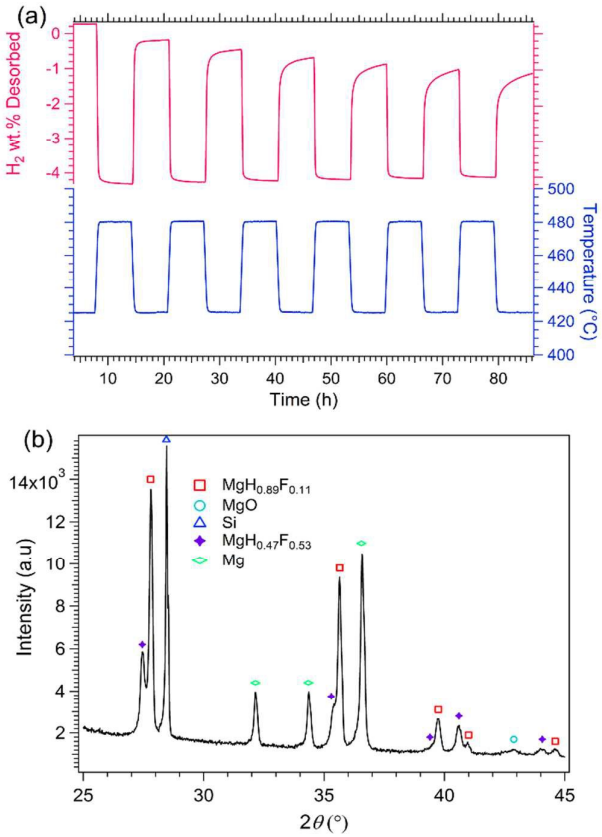

Fig. 7. (a) Cycling studies of $Mg(H_{0.85}F_{0.15})_2$; (b) XRD after cycling in the hydrogenated state. λ = 1.5418 Å, at room temperature.

end of the absorption PCI, quantitative Rietveld refinement of the XRD data shows that two compositions of $Mg(H_xF_{1-x})_2$ are identified, although due to the asymmetry of the peaks there are maybe a larger distribution of compositions (Fig. 6c). The compositions are determined, based on the unit cell volume method (Fig. 2b), to be approximately 90 wt% $Mg(H_{0.86}F_{0.14})_2$ and 10 wt% $Mg(H_{0.56}F_{0.44})_2$. Macroscopic flakes are evident in the rehydrogenated sample when visually inspected, which are attributed to the sintering of the material at high temperature. This was previously reported by Bogdanovic *et al.*[52] by observing that Mg metal agglomerates during and is likely to be responsible for the reduced kinetics.[14]

Cycling studies

The cyclability of $Mg(H_{0.85}F_{0.15})_2$-*S* was investigated to characterise its long-term reversibility and its potential use in technological applications. Cycling studies were conducted over six absorption/desorption cycles between 480 °C (desorption) and 425 °C (absorption) (Fig. 8a). A system pressure of ~27 bar was utilised to ensure full absorption and desorption could occur during the cycling studies. Over the course of the 6 consecutives absorption/desorption cycles, the

View Article Online
DOI: 10.1039/C7CP07433F

hydrogen capacity of the sample decreased gradually, as seen in Fig. 8a. For these conditions, the hydride desorbed 4.6 wt% H_2 for the first desorption with ~92% of hydrogen being desorbed after ~35 min. The sample then absorbed 4.08 wt% H_2 with 97 % being absorbed in less than 30 min. After the first cycle, the capacity of $Mg(H_{0.85}F_{0.15})_2$ was reduced by 19 % and over the 6 cycles the sample lost a total of ~27 % capacity. Sintering of the Mg in the sample is responsible for the decrease in capacity (clearly impacting kinetics) and was confirmed by visual observation of flakes inside the sample after cycling. The cycling measurement was stopped after absorption, at which point XRD was undertaken (Fig. 8b). Quantitative analysis shows that two $Mg(H_xF_{1-x})_2$ phases were present, both of which are H-rich, along with Mg metal, confirming what was previously observed in the absorption stage of the PCI experiment. The main phase is $Mg(H_{0.89}F_{0.11})_2$ and the other is $Mg(H_{0.47}F_{0.53})_2$.

Conclusions

A range of $Mg(H_xF_{1-x})_2$ (x = 1, 0.95, 0.85, 0.70, 0.50, 0) solid solutions have being synthesised by ball milling quantitative ratios of MgH_2 and MgF_2 followed by annealing under a hydrogen backpressure. Their potential use as hydrogen storage or thermal energy storage materials has been examined by *in situ* synchrotron XRD, DSC-TGA-MS and PCI analysis. Thermal studies were carried out on all $Mg(H_xF_{1-x})_2$ mixtures concluding that increased F content increases the thermal stability and decreases the absorption/desorption kinetics compared to pure MgH_2. As such, decomposition occurs in a single step with DSC data showing a maximum rate of H_2 desorption at 434 °C for $Mg(H_{0.85}F_{0.15})_2$, with a practical hydrogen capacity of 4.6 ± 0.2 H_2 wt% (theoretical 5.4 wt% H_2). An extremely stable $Mg(H_{0.43}F_{0.57})_2$ phase is formed upon the decomposition of each Mg–H–F composition of which the remaining H_2 is not released until after 505 °C. PCI measurements of $Mg(H_{0.85}F_{0.15})_2$ determined an enthalpy of decomposition of 73.6 ± 0.2 kJ/mol H_2 and an entropy of 131.2 ± 0.2 J/K/mol H_2. In comparison with MgH_2, these values are decreased from 74.06 kJ/mol H_2 and 133.4 J/K/mol H_2, respectively.[14] Cycling of $Mg(H_{0.85}F_{0.15})_2$ has been investigated over six cycles between 420 and 480 °C, with a reduction of 27 % of the practical hydrogen capacity of 4.6 wt% H_2. This represents an increased cycling temperature of ~80 °C compared to bulk MgH_2 which increases the thermal operating temperatures for technological applications, thereby increasing efficiency.

Conflicts of interest

There are no conflicts to declare.

Acknowledgements

CEB, DAS and MP acknowledge the financial support of the Australian Research Council (ARC) for ARC Linkage grants LP120101848 and LP150100730, and CEB acknowledges the financial support of the ARC LIEF grants LE0775551 and LE0989180, which enabled the XRD and gas absorption/desorption measurements to be undertaken. DAS acknowledges the financial support of a Curtin University Postdoctoral Research Fellowship and MP acknowledges his ARC Future Fellowship FT160100303. The authors also acknowledge funding from the Australian Synchrotron (ANSTO), which enabled the research at the powder diffraction beamline to be undertaken.

References

1 M. Paskevicius, L. H. Jepsen, P. Schouwink, R. Černý, D. B. Ravnsbæk, Y. Filinchuk, M. Dornheim, F. Besenbacher and T. R. Jensen, *Chem. Soc. Rev.*, 2017, **46**, 1565-1634.
2 R. Mohtadi and S.-i. Orimo, *Nat. Rev. Mater.*, 2016, **2**, 16091.
3 S.-i. Orimo, Y. Nakamori, J. R. Eliseo, A. Züttel and C. M. Jensen, *Chem. Rev.*, 2007, **107**, 4111-4132.
4 K. T. Møller, D. Sheppard, D. B. Ravnsbæk, C. E. Buckley, E. Akiba, H.-W. Li and T. R. Jensen, *Energies*, 2017, **10**, 1645.
5 D. A. Sheppard, M. Paskevicius, T. D. Humphries, M. Felderhoff, G. Capurso, J. Bellosta von Colbe, M. Dornheim, T. Klassen, P. A. Ward, J. A. Teprovich, C. Corgnale, R. Zidan, D. M. Grant and C. E. Buckley, *Appl. Phys. A*, 2016, **122**.
6 D. N. Harries, M. Paskevicius, D. A. Sheppard, T. Price and C. E. Buckley, *Proc. IEEE*, 2012, **100**, 539-549.
7 J. F. Stampfer, C. E. Holley and J. F. Suttle, *J. Am. Chem. Soc.*, 1960, **82**, 3504-3508.
8 D. L. Douglass, *Metall. Mater. Trans. A*, 1975, **6**, 2179.
9 Q. Lai, M. Paskevicius, D. A. Sheppard, C. E. Buckley, A. W. Thornton, M. R. Hill, Q. Gu, J. Mao, Z. Huang, H. K. Liu, Z. Guo, A. Banerjee, S. Chakraborty, R. Ahuja and K.-F. Aguey-Zinsou, *ChemSusChem*, 2015, **8**, 2789-2825.
10 J. C. Crivello, R. V. Denys, M. Dornheim, M. Felderhoff, D. M. Grant, J. Huot, T. R. Jensen, P. de Jongh, M. Latroche, G. S. Walker, C. J. Webb and V. A. Yartys, *Appl. Phys. A*, 2016, **122**, 85.
11 T. D. Humphries, D. A. Sheppard and C. E. Buckley, *Coord. Chem. Rev.*, 2017, **342**, 19-33.
12 J. Komiyama, K. Eriguchi, Y. Abe, S. Suzuki, H. Nakanishi, T. Yamane, H. Murakami and A. Koukitu, *J. Cryst. Growth*, 2008, **310**, 96-100.
13 D. A. Sheppard, T. D. Humphries and C. E. Buckley, *Appl. Phys. A*, 2016, **122**, 406.
14 M. Paskevicius, D. A. Sheppard and C. E. Buckley, *J. Am. Chem. Soc.*, 2010, **132**, 5077-5083.
15 M. Wierse, R. Werner and M. Groll, *J. Less-Common Met.*, 1991, **172**, 1111-1121.
16 B. Bogdanović and B. Spliethoff, *Int. J. Hydrogen Energy*, 1987, **12**, 863-873.
17 B. Bogdanovic, B. Spliethoff and A. Ritter, *Z. Phys. Chem. Neue Fol.*, 1989, **164**, 1497-1508.
18 B. Bogdanović, T. H. Hartwig and B. Spliethoff, *Int. J. Hydrogen Energy*, 1993, **18**, 575-589.
19 B. Bogdanovic, A. Ritter and B. Spliethoff, *Int. J. Hydrogen Energy*, 1995, **20**, 811-822.
20 M. Paskevicius, D. A. Sheppard, K. Williamson and C. E. Buckley, *Energy*, 2015, **88**, 469-477.
21 D. Dong, T. D. Humphries, D. A. Sheppard, B. Stansby, M. Paskevicius, M. V. Sofianos, A. L. Chaudhary, M. Dornheim and C. E. Buckley, *Sus. Energy Fuels*, 2017, **1**, 1820-1829.
22 W. E. Wentworth and E. Chen, *Solar Energy*, 1976, **18**, 205-214.

View Article Online
DOI: 10.1039/C7CP07433F

23 *SunShot Vision Study, Chapter 5: Concentrating Solar Power Technologies, Cost, and Performance*, US Department of Energy, 2012.
24 P. A. Ward, C. Corgnale, J. A. Teprovich, T. Motyka, B. Hardy, D. Sheppard, C. Buckley and R. Zidan, *Appl. Phys. A*, 2016, **122**, 462.
25 M. Felderhoff and B. Bogdanovic, *Int J Mol Sci*, 2009, **10**, 325-344.
26 D. A. Sheppard, T. D. Humphries and C. E. Buckley, *Mater. Today*, 2015, **18**, 414-415.
27 T. D. Humphries, D. A. Sheppard, M. R. Rowles, M. V. Sofianos and C. E. Buckley, *J. Mater. Chem. A*, 2016, **4**, 12170-12178.
28 D. A. Sheppard, C. Corgnale, B. Hardy, T. Motyka, R. Zidan, M. Paskevicius and C. E. Buckley, *RSC Adv.*, 2014, **4**, 26552-26562.
29 P. A. Ward, C. Corgnale, J. A. Teprovich, T. Motyka, B. Hardy, B. Peters and R. Zidan, *J. Alloys Compd.*, 2015, **645**, S374-S378.
30 S. Deledda, A. Borissova, C. Poinsignon, W. J. Botta, M. Dornheim and T. Klassen, *J. Alloys Compd.*, 2005, **404**, 409-412.
31 A. R. Yavari, A. LeMoulec, F. R. de Castro, S. Deledda, O. Friedrichs, W. J. Botta, G. Vaughan, T. Klassen, A. Fernandez and A. Kvick, *Scr. Mater.*, 2005, **52**, 719-724.
32 P. Jain, V. Dixit, A. Jain, O. Srivastava and J. Huot, *Energies*, 2015, **8**, 12330.
33 L.-P. Ma, P. Wang and H.-M. Cheng, *Int. J. Hydrogen Energy*, 2010, **35**, 3046-3050.
34 I. E. Malka, M. Pisarek, T. Czujko and J. Bystrzycki, *Int. J. Hydrogen Energy*, 2011, **36**, 12909-12917.
35 S. A. Pighin, G. Urretavizcaya and F. J. Castro, *Int. J. Hydrogen Energy*, 2015, **40**, 4585-4596.
36 S. A. Pighin, G. Urretavizcaya and F. J. Castro, *J. Alloys Compd.*, 2017, **708**, 108-114.
37 K. S. Wallwork, B. J. Kennedy and D. Wang, 2007.
38 P. Pathak and N. Vasavada, *Acta Crystallogr. A*, 1970, **26**, 655-658.
39 I.-K. Suh, H. Ohta and Y. Waseda, *J. Mater. Sci.*, 1988, **23**, 757-760.
40 G. Vidal-Valat, J.-P. Vidal, C. M. Zeyen and K. Kurki-Suonio, *Acta Crystallogr., Sect. B: Struct. Sci.*, 1979, **35**, 1584-1590.
41 F. H. Ellinger, C. E. Holley, B. B. McInteer, D. Pavone, R. M. Potter, E. Staritzky and W. H. Zachariasen, *J. Am. Chem. Soc.*, 1955, **77**, 2647-2648.
42 C. E. Messer, *J. Solid State Chem.*, 1970, **2**, 144-155.
43 M. Polanski, T. Płociński, I. Kunce and J. Bystrzycki, *Int. J. Hydrogen Energy*, 2010, **35**, 1257-1266.
44 B. Bogdanović, A. Reiser, K. Schlichte, B. Spliethoff and B. Tesche, *J. Alloys Compd.*, 2002, **345**, 77-89.
45 I. Almaz Optics, Almaz Optics, Inc., http://www.almazoptics.com/MgF2.htm, (accessed 03/11/2017, 2017).
46 E. CDS, 316 Stainless Steel Mechanical Properties, https://www.ezlok.com/technical-info/mechanical-properties/316-stainless-steel, (accessed 03/11/2017, 2017).
47 W. H. Baur, *Acta Crystallogr., Sect. B: Struct. Sci.*, 1976, **32**, 2200-2204.
48 T. Noritake, M. Aoki, S. Towata, Y. Seno, Y. Hirose, E. Nishibori, M. Takata and M. Sakata, *Appl. Phys. Lett.*, 2002, **81**, 2008-2010.
49 M. Polanski, T. K. Nielsen, Y. Cerenius, J. Bystrzycki and T. R. Jensen, *Int. J. Hydrogen Energy*, 2010, **35**, 3578-3582.
50 S. S. S. Raman, D. J. Davidson, J. L. Bobet and O. N. Srivastava, *J. Alloys Compd.*, 2002, **333**, 282-290.
51 W. Klostermeier and E. U. Franck, *Ber Bunsen Phys Chem*, 1982, **86**, 606-612.
52 B. Bogdanovic, H. Hofmann, A. Neuy, A. Reiser, K. Schlichte, B. Spliethoff and S. Wessel, *J. Alloys Compd.*, 1999, **292**, 57-71.